Global Positioning System Measurements of Crustal Deformation in the Taiwan Arc-Continent Collision Zone

SHUI-BEIH YU[1] and HORNG-YUE CHEN[1]

ABSTRACT

A 78-station 270 km wide Global Positioning System (GPS) network which spans the arc-continent collision zone in southern Taiwan has been surveyed 5 times from 1990 to 1994 with dual-frequency geodetic GPS receivers. The observed data are processed with Bernese software, v.3.4, using the available precise ephemerides. The unknown residual tropospheric zenith delays are estimated once per 6-8 hour session for each station in the least squares adjustment of carrier phase observations. The standard errors of GPS observed lengths are in the range of 5 to 9 mm for a baseline of 3-120 km in length. The changes in baseline length are utilized to study the spatial variations of crustal strain and estimate the relative velocities of geodetic stations. We found that the deformation zone caused by the active collision process is probably 200 km in width. The Coastal Plain, eastern part of the Western Foothills, Central Range, and Coastal Range show slight to moderate strain rates. Remarkable contractions of 0.51-1.65 μstrain/yr in 100°-120° are detected in the vicinity of the Chukou fault. The Longitudinal Valley gives extremely high shortening rates of 3.2-6.1 μstrain/yr in 109°-133°. It is obvious due to the aseismic slip on the Longitudinal Valley fault as previously demonstrated by trilateration data. The velocity field of GPS stations reveals a fan-shaped pattern consistent with the directions of maximum compressional tectonic stress inferred from borehole breakout data, earthquake focal mechanisms, and Quaternary geological data. The GPS observed velocity of Lanhsu on the Luzon arc relative to Paisha, Penghu of the Chinese continental margin, 86.3±2.4 mm/yr in 307°±1°, is almost in the same direction as that proposed by Seno (1977) or Seno et al. (1993), but the rate is about 15-20% faster.

(Key words: GPS survey, Crustal strain, Velocity field, Arc-continent collision)

---

[1] Institute of Earth Sciences, Academia Sinica, P.O. Box 1-55, Nankang, Taipei, Taiwan, R.O.C.

1. INTRODUCTION

Highly active seismicity and rapid crustal movement have been observed in the Taiwan area (e.g., Tsai *et al.*, 1977; Wu, 1978; Tsai, 1986; Yu and Tsai, 1982; Yu and Lee, 1986). These phenomena are obviously the consequence of the plate interaction (subduction and collision) between the Philippine Sea and Eurasian plates. Using a large number of reliably located earthquake data, Tsai *et al.* (1977) pointed out a north-dipping Benioff zone under northeasten Taiwan. This is strong evidence to support the northward subduction of the Philippine Sea plate underneath the Eurasian plate near 24°N. Tsai (1986) further recognized an east-dipping Benioff zone of about 30 km in thickness which begins to deepen along 121°E at a dip angle of 55°-60° toward east. The leading edge of the Benioff zone reaches a depth of about 180 km between 21°N and 22°N but tapers off to a shallower depth of about 100 km from 22°N to 23°N which implies that the subduction of the South China Sea under the Philippine Sea plate extends from Luzon northward until about 23°N.

Based on the analysis of the repeated trilateration and leveling data in the Longitudinal Valley area in eastern Taiwan from 1983 to 1989, it was found that the 50 km long central segment of the Longitudinal Valley Fault (hereafter referred as LVF) is creeping significantly (Yu and Liu, 1989). The eastern side of the LVF belonging to the Coastal Range is steadily uplifting at a maximum rate of about 20 mm/yr relative to the western side belonging to the Longitudinal Valley. In the Taitung area of the southernmost Longitudinal Valley, the relative vertical movement across the LVF is not appreciable (Yu *et al.*, 1992). Using a 3-dimensional dislocation model and the Bayesian non-linear inversion method (Jackson and Matsu'ura, 1985), the repeated geodetic data are inverted to estimate some fault parameters of the LVF and the block velocities on both sides of the fault (Yu *et al.*, 1990). It is concluded that the LVF is weakly locked, and the aseismic fault slip is predominant. The relative horizontal block velocities between the Coastal Range and the Central Range are 28-31 mm/yr (Yu and Yu, 1991) which reveals that about 40% of the 70 mm/yr plate convergence by Seno (1977) is taken up on a quite narrow zone of only a few kilometers in width centered on the LVF.

Being limited by the capability of the electronic distance meter (EDM) which was used in the trilateration surveys (measuring range < 10 km) and the hard accessible mountainous terrain, the trilateration networks for observing horizontal deformation in the Longitudinal Valley area all have small apertures with widths of only 5-10 km. Based on the observations from these small networks, therefore the total width of the deformation zone caused by the active collision between the Luzon arc and Chinese continental margin cannot be determined. Using the earthquake slip vector data along the plate boundary and the constraint from the global relative plate model NUVEL-1 (DeMets *et al.*, 1990), Seno (1977) and Seno *et al.* (1993) estimate the velocity of the Philippine Sea plate relative to the Eurasian plate in the vicinity of Taiwan to be 70-73 mm/yr in 309°. This figure has been widely quoted in the interpretation of geological observations or modeling in the Taiwan area (e.g. Suppe, 1981, Lu and Malavieille, 1994). Whether Seno's estimation of the relative plate motion is accurate enough or not, needs to be studied and verified. With the traditional geodetic survey methods (triangulation or trilateration), it is difficult to largely expand the original trilateration networks to cover the whole collision zone so that the width of the deformation zone can be resolved and thus Seno's estimation be verified. Fortunately, the newly developed Global Positioning System (GPS) survey technique provides a good opportunity to solve the previous problem shortcomings.

The Global Positioning System is a satellite-based navigation system operated by the U.S. Department of Defense. It consists of a constellation of 24 satellites in orbits of 20,000

km in altitude, with orbital periods of about 12 hr. At least four satellites are visible simultaneously at all times from almost anywhere on Earth. With the carrier phase signals from GPS satellites being received and processed at two or more sites simultaneously, the 3-dimensional relative position of these sites can be precisely determined. Unlike the traditional survey techniques, the GPS survey does not require the line-of-sight intervisibility of geodetic monuments. It is much less affected by rugged topography and bad weather conditions. Thus, an optimal GPS network can easily be designed to monitor the crustal deformation in the studied area.

In 1989 a large scale "Taiwan GPS Network" was established by the Institute of Earth Sciences, Academia Sinica. This network is composed of 140 stations and covers the whole island of Taiwan as well as five offshore islets. The southern half of the network has been surveyed 5 times during the period from 1990 to 1994 (Figure 1). This subnetwork includes 78 stations and extends from two islets, Paisha and Chimei, in the geologically
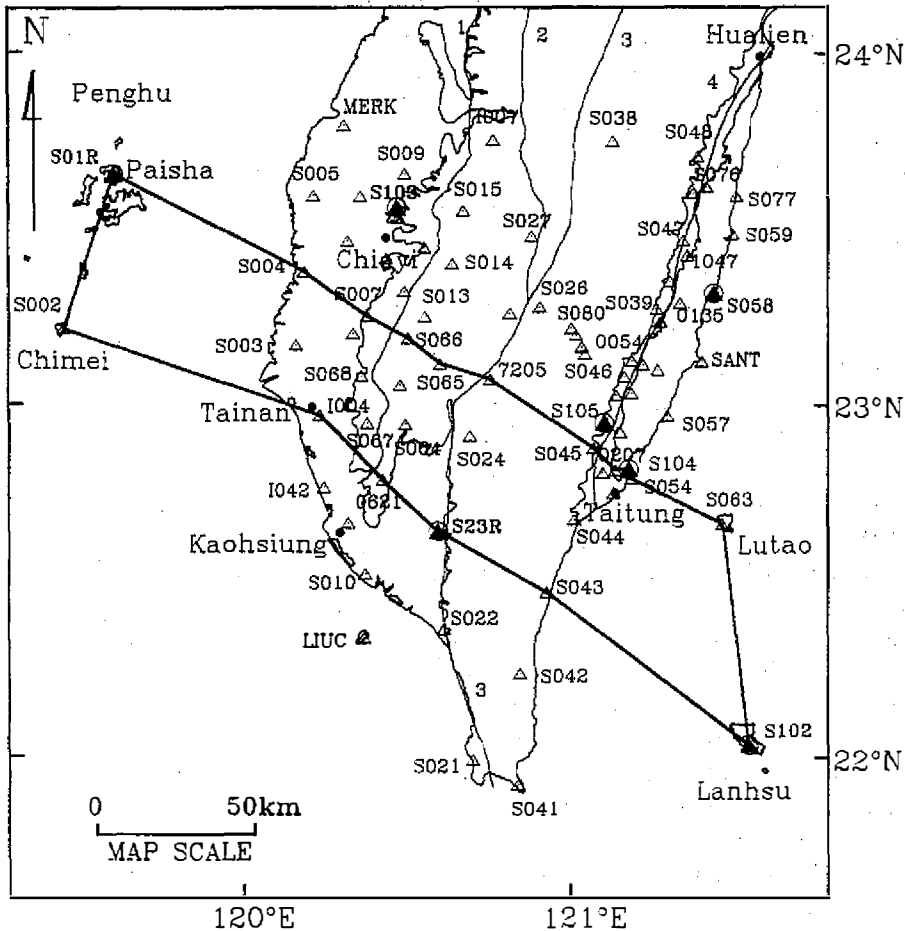

Fig. 1. The southern Taiwan GPS Network. Blank triangles are GPS stations surveyed annually, while the solid triangles inside circles are continuous-monitoring fixed stations. The thick lines are the major faults. 1. Chukou fault, 2. Chenyulanchi fault, 3. Lishan-Chaochou fault, 4. Longitudinal Valley fault. Two NW-SE profiles are also shown.

stable Penghu Islands southeasterly to the two volcanic islands of Luzon arc, Lutao and Lanhsu, offshore of Taitung. This 270 km wide GPS network is likely to cover the entire arc-continent collision zone in Taiwan. The changes in the baseline vectors obtained from these repeated GPS surveys are utilized to study the crustal deformation in the active Taiwan collision zone. In this paper we describe the field procedures of the GPS surveys and the strategy of postprocessing. The precision of the GPS observations here is evaluated and the spatial variations of the strain accumulation rates in the different geologic provinces are studied. Additionally, the velocity field of the geodetic stations is estimated, and its tectonic implication is discussed.

2. GEOLOGICAL SETTING

The island of Taiwan is situated on a convergent boundary between the Philippine Sea plate and Eurasian plate (Figure 2a). The Philippine Sea plate subducts northward beneath the Eurasian plate at the Ryukyu Trench and overrides the crust of the South China Sea at the Manila Trench. The southeast facing Ryukyu arc-trench system extends from southern Kyushu of Japan to the east of Taiwan near 123°E. The west-facing Luzon arc-Manila Trench system extends from the Philippines to about 22°N off southwestern Taiwan. Between the two opposite-facing Ryukyu and Luzon arcs, the Longitudinal Valley in eastern Taiwan is widely considered the suture zone of the collision between the Luzon arc and the Chinese continental margin (e.g., Big, 1972; Hsu, 1976; Bowin *et al.*, 1978; Wu, 1978; Barrier and Angelier, 1986; Ho, 1986).

Taiwan is generally divided into several tectonostratigraphic belts (Ho, 1982, 1986) which trend mainly north-northeast (Figure 2b). From west to east they are: the Coastal Plain, Western Foothills, Central Range, Longitudinal Valley and the Coastal Range. The Coastal Plain consists of Quaternary alluvial deposits derived from the Central Range and the Western Foothills. The Neogene sediments underneath the alluvial cover have a regional dip toward the east. The Western Foothills are composed of a thick sequence of shallow marine to shelf clastic sediments from the late Oligocene, Miocene, to early Pleistocene (Huang, 1978 and 1980). The rocks in the Western Foothills were deformed by a combination of folds and thrust faults which trend mainly northeast or north and dip toward the east or southeast (Ho, 1976; Suppe, 1980). The Central Range is divided into two parts. The western flank and high ridges of the Central Range are underlain by a weakly metamorphosed Cenozoic argillite-slate series. Based on the differences in lithology and in grade of metamorphism, this argillite-slate belt is further divided into two zones, the Hsuehshan Range and the Backbone Range. The eastern flank of the Central Range is composed of the pre-Tertiary basement complex which has been affected by Neogene greenshist facies and higher grades of polyphase Mesozoic-Cenozoic metamorphism.

The Coastal Range and the two offshore islets, Lutao and Lanhsu, are the northern extension of the Neogene Luzon volcanic arc and the forearc basin of the North Luzon Trough. The structure of the Coastal Range is characterized by low-angle east-dipping imbricate thrust faults and longitudinal NNE-trending anticlines and synclines. The straight and narrow Longitudinal Valley lies between the Central Range and the Coastal Range. It is bounded on the east by the well-known Longitudinal Valley Fault (LVF) with the Coastal Range. The LVF is a high-angle oblique thrust fault with a minor left-lateral strike-slip component (Barrier *et al.*, 1982).
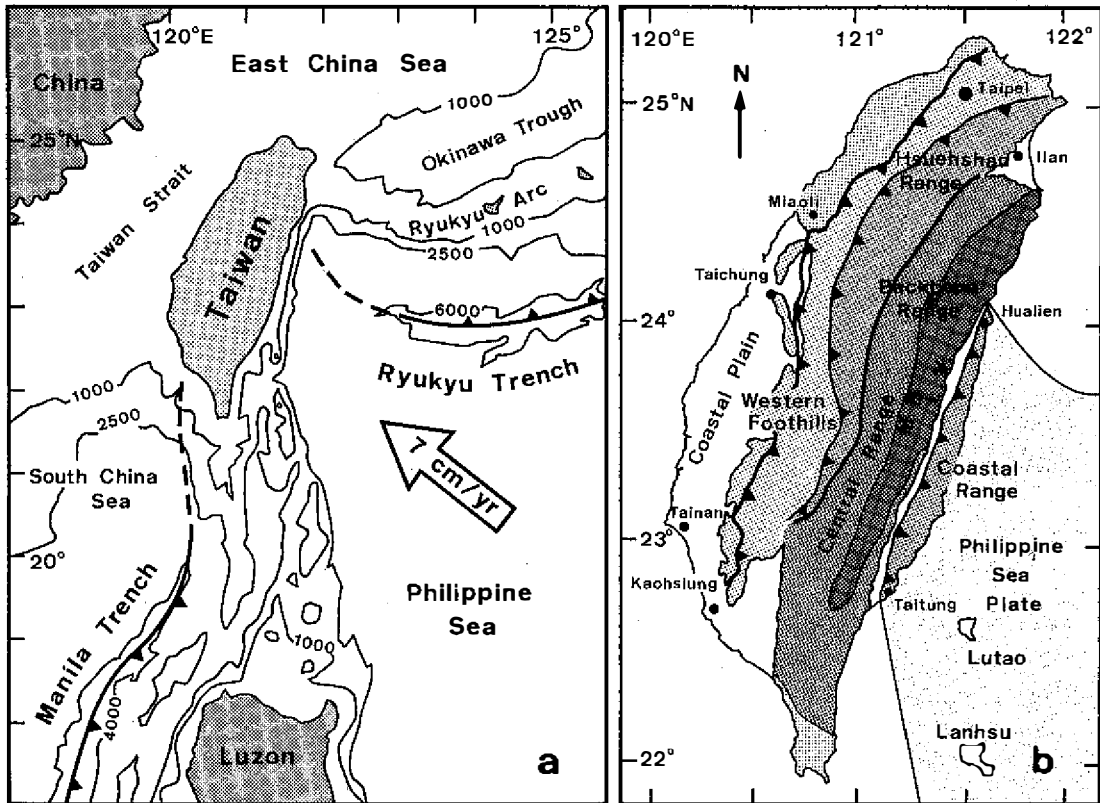
Fig. 2. Location map and main tectonic units in Taiwan. (a) Geodynamic frame-
work: isobaths in meters, large open arrow showing the present direction
of convergence (Philippine Sea plate relative to Eurasia). Thick lines with
triangles barb as subduction; barbs on overriding side. (b) Tectonic frame-
work and structural units: major thrust faults as heavy lines with triangles
on the upthrust side. L. V., Longitudinal Valley; M. B., Metamorphic
Basement (after Ho, 1986 and Hu *et al.*, 1994).

3. FIELD WORK AND DATA PROCESSING

The southern Taiwan GPS Network consists of 78 stations which are generally located
at geologically stable sites with good sky visibility for elevation angles larger than 15 degrees.
Five epoch measurements of the network were carried out during the periods of March to
July, 1990, June to August, 1991, May to July, 1992, May to June, 1993, and January to
March, 1994. In each survey 4-8 stations are observed simultaneously with mobile geodetic
dual-frequency GPS receivers (Model: Trimble 4000 SST Geodetic IIP). A station is usually
occupied longer than two sessions. A session is composed of a 6-8 hour GPS observation with
more than 9 satellites being tracked. The sampling interval for data logging is 15 seconds,
and only those signals from satellites with elevation angles larger than 15° are recorded. The
collected field data are downloaded from the internal RAM of receivers to PC hard disks
or floppy disks. The raw data of each station are then transfered to the RINEX (Receiver

INdependent EXchange) format by a transfer program. The raw data and that transfered to the RINEX format of all stations are stored in two separate 650 MB optical disks for long-term preservation.

Major error sources for GPS positioning include clock biases in both the satellite and ground receiver, the frequency-dispersive ionosphere (50-500 km altitude) and the nondispersive troposphere (0-10 km altitude) delays of signal, uncertainties in the satellite position at the time of signal transmission and carrier phase cycle ambiguities (Dixon, 1991). Relative GPS positioning involves the simultaneous observation of a group of satellites by a network of ground receivers. It allows cancellation of variations in the receiver's oscillators by differencing the carrier phase received simultaneously from two or more satellites. The phase received from a given satellite by two or more receivers can also be differenced to cancel the effects of the satellite oscillator. Thus, the double differenced phase measurements allow for the elimination of the variations of both transmitter and receiver oscillators, and also greatly reduce the other errors listed above, resulting in the milimeter- to centimeter- level position data for crustal deformation studies.

The Bernese software v.3.4 developed at the Astronomical Institute of the University of Berne, Switzerland is employed in the postprocessing of the observed GPS data. We process the data in each survey session by session and obtain the baseline solutions for all combinations of the two stations in the same observation session. In 1990 and part of 1991 surveys broadcast ephemerides are used in the processing. The precise ephemerides provided by the Scripps Institution of Oceanography of the University of California, San Diego, U.S.A. (SIO) and the International GPS Service for Geodynamics (IGS) are utilized in the postprocessing of 1992-1994 data. The precision in orbit estimates by SIO or the IGS is better than 50 cm (Goad, 1993). Thus, for a baseline of less than 100 km in length, the error due to orbit is less than 2 mm.

The effects of the dispersive ionospheric delay can be reduced to a milimeter or less by combining observations at the L1 and L2 frequencies in such a way that first-order ionospheric effects are removed. This linear combination is termed ionosphere-free observable, or L3. An elevation cutoff angle of 20° is used to reduce any multipath effects. The modified Hopfield (1971) atmospheric zenith delay model with standard atmosphere are employed to calculate an a priori model for tropospheric correction. The standard atmospheric model usually fails to describe the actual meteorological conditions at a GPS station during a particular observation session (Brunner and Welsch, 1993). The difference between the actual zenith delay and that calculated from a standard atmospheric model is called the residual zenith delay. We estimate the unknown residual zenith delay once per 6-8 hour observation session for each station in the least-squares adjustment of the carrier phase observations. Kuo *et al.* (1994) noted that this estimation process can effectively improve the precision of the vertical component. The phase ambiguities are firstly estimated as real numbers and then fixed to as many of the closest integers as possible. Usually more than 90% of the ambiguities are fixed for each session.

4. PRECISION OF GPS MEASUREMENT

Based on the propagation of random data noise through the estimation process, the formal error can be one measure of the uncertainty of a GPS baseline estimate (Dixon, 1991). Since it does not account for all random errors nor most systematic errors, the formal error usually underestimates the true error. For instance, Willams *et al.* (1993) noticed that

the formal variance computed by the GPS estimation program underestimates the standard errors by a factor of 8 to 11.

The scatter of daily solutions for a GPS experiment spanning several days is one indicator of GPS precision. This short-term repeatability has been used to assess the relative merits of various experimental and analytical approaches (e.g. Tralli and Dixon, 1988; Dong and Bock, 1989; Blewitt, 1989). However, the slowly varying systematic errors due to propagation delay, multipath, or fiducial network inconsistencies, and so forth may not be revealed by short-term repeatability. Since the GPS data here span the four year period from 1990 to 1994, we use the scatter of a series of GPS measurements taken over years as the indicator of precision. This long-term repeatability shows the effects of slowly varying errors.

We assume steady motion between stations during the four-year period and look at the scatter of data points about a best fit straight line on a plot of the baseline component versus time (Davis *et al.,* 1989). The repeatability R of a baseline component (east, north, or vertical) or baseline length is the weighted root-mean-square scatter about the linear trend :

$$R = \left[\frac{\frac{n}{n-2} \sum_{i=1}^{n} \frac{(c_i - \hat{c}_i)^2}{\sigma_i^2}}{\sum_{i=1}^{n} \frac{1}{\sigma_i^2}} \right]^{1/2} \qquad (1)$$

where n is the number of surveys, c_i is the estimate of the component or length of a baseline on the i th survey, σ_i is the formal error, and $\hat{c}_i$ is the linear estimate at the time of the i th survey, t_i:

$$\hat{c}_i = c_0 + r \cdot t_i \qquad (2)$$

where c_0 is the estimated origin value of component c at t=0, and r is the linear rate of change for that component.

Figure 3 shows the plots of repeatabilities of length and north, east, and vertical components for all baseline vectors used in this study versus baseline length. The baselines range from 3 to 120 km in length with the majority less than 50 km. The overall precision of an individual GPS baseline estimate depends on several factors, whose contribution to the total are the square root of the summed squares of the individual error terms (Dixon, 1991). Some of these errors are constant, while others depend on baseline length. The formalism proposed by Savage and Prescott (1973) is employed here to describe the precision of the GPS measurements as a function of baseline length :

$$\sigma_L = \left(a^2 + b^2 \cdot L^2 \right)^{1/2} \qquad (3)$$

where σ_L is the standard deviation, L is the baseline length, a and b are the constant and length-dependent sources of error, respectively. Best fitting curves (3) through the repeatability data shown in Figure 3 give a=5.4±0.2 mm, 5.0±0.2 mm, 6.6±0.3 mm, 22.1±1.1 mm, and b=0.06±0.01 ppm, 0.07±0.01 ppm, 0.09±0.02 ppm, 0.31±0.04 ppm for length and north, east, and vertical components respectively. This means the standard deviations range from 5-9 mm in length, 5-10 mm on the north component, 7-13 mm on the east component, and 22-43 mm on the vertical component for baseline lengths in the range of 3 to 120 km. The east component is determined a little more poorly than the north component.

Since the satellite ground tracks are oriented mainly north-south, giving large range-change signals in the north-south direction. With mostly phase ambiguity-fixed data, the difference in precision on the east and north components has been reduced. The vertical component is the most poorly determined with GPS. In this case, it is 3-4 times worse than the horizontal components. This reflects the inherent geometric limitation that satellites are observed in the upper hemisphere only and higher sensitivity to errors in tropospheric calibration (Herring, 1986).
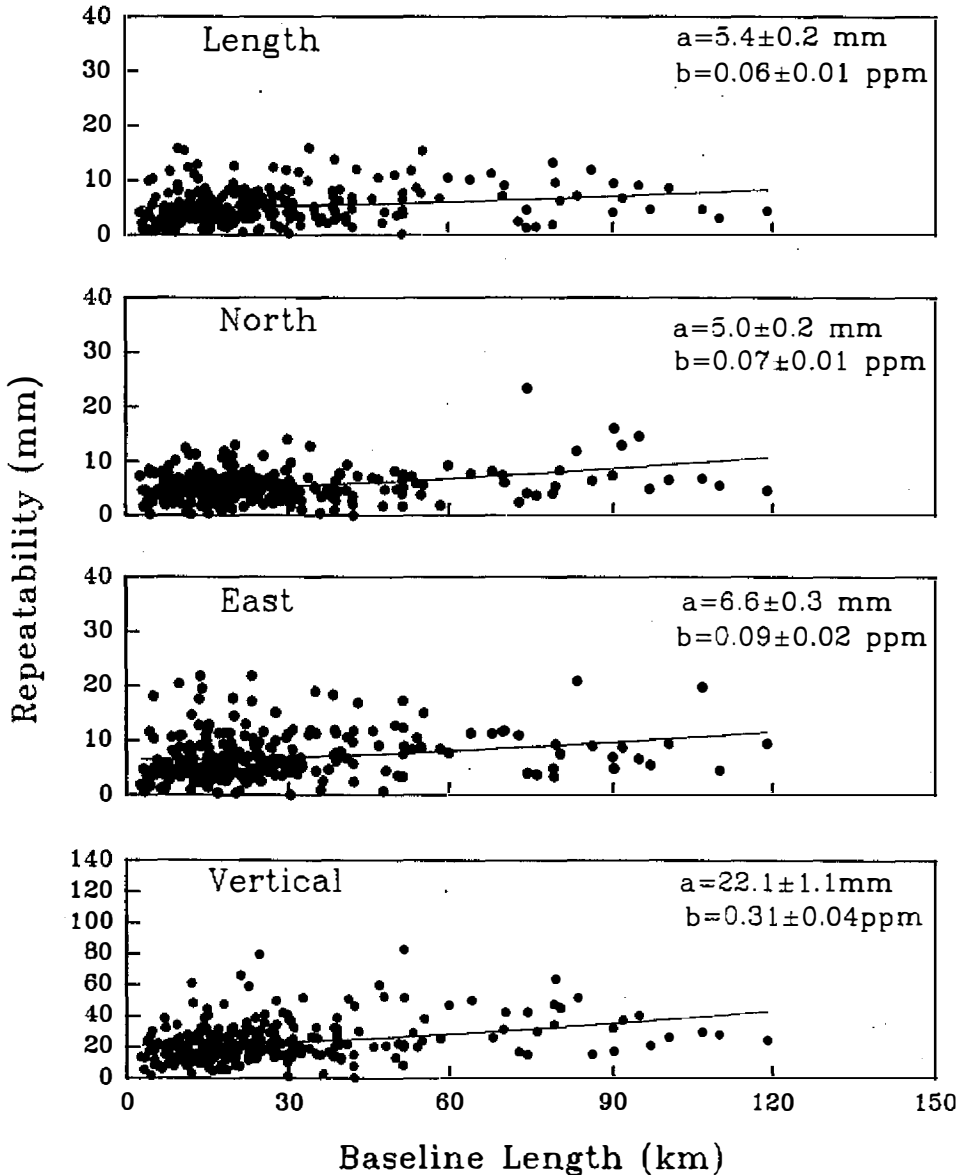

Fig. 3. Long-term repeatability for all baselines in the southern Taiwan GPS Network. Curves are best fit (Equation (3)) through each component.

5. SPATIAL VARIATION OF CRUSTAL STRAIN

As mentioned previously, the vertical precision of GPS measurement is much worse than its horizontal precision; thus, it is still not good enough for detecting the minute vertical crustal deformation within a short time period of less than four years. In this study only the changes in baseline lengths from the repeated GPS surveys are used to assess the spatial variation of the horizontal crustal strain over the arc-continent collision zone. Based on the geologic features and the distribution of geodetic stations, the southern Taiwan GPS Network is divided into 22 subnets denoted by capital letters from A to V (see Figure 4). From west to east, Net A includes the offshore area between the Penghu Islands and the southwestern coast of Taiwan, Nets B and C are the Coastal Plain, Nets D, E, F, and G cover the vicinity of the Chukou fault. Nets H, I, J, and K include the eastern part of the Western Foothills, a small portion of the western Central Range and the Pingtung plain. Nets L, M, N, and O belong to the Central Range and the Hengchun Peninsula. The narrow and elongated Nets P, Q, and R are the Longitudinal Valley. Nets S, T, and U cover the Coastal Range and a part of the eastern offshore area. Net V is the large offshore area between Lutao-Lanhsu and the southeastern coast of Taiwan.
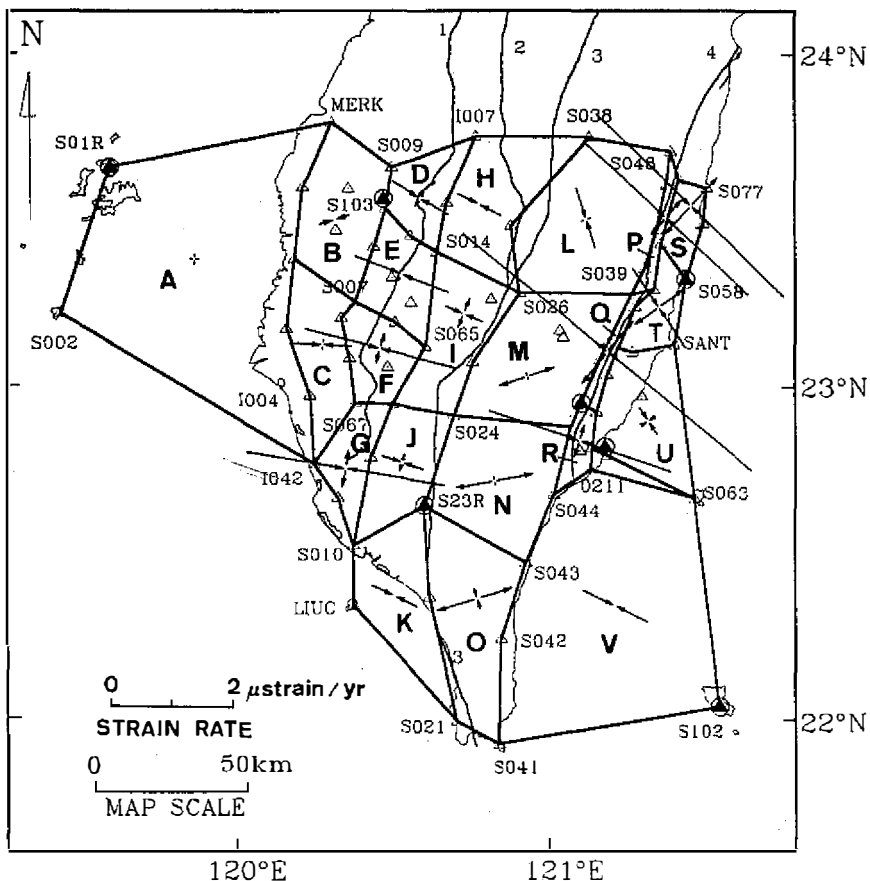

Fig. 4. Average principal strain rates of 22 subnets. The scale of strain rates at Nets P, Q, R are reduced to half.

It is assumed that, spatially, the crustal strain accumulates uniformly over each subnet shown in Figure 4, and the rate of strain accumulation is constant over the time period of 1990-1994. Following the procedures of Prescott *et al.* (1979), the average annual strain rate of each net can be calculated. The strain rate for each baseline, $\dot{e}$, is expressed as, $\dot{e} = L^{-1}(dL/dt)$, where L is the baseline length and dL/dt is the average rate of length change. $\dot{e}$ is related to the surface strain rate tensor, $\dot{E}_{ij}$, by:

$$\dot{e} = \dot{E}_{11}\ sin^2\theta + \dot{E}_{12}\ sin2\theta + \dot{E}_{22}\ cos^2\theta \qquad (4)$$

where θ is the azimuth (measured clockwise from the north) of the baseline and the strain rate tensor is referred to a geographic coordinate system with the axis 1 directed east and axis 2 directed north. Three components of average strain rate tensor, $\dot{E}_{11}$, $\dot{E}_{12}$, and $\dot{E}_{22}$, calculated using all of the surveys for each of the 22 subnets are given in Table 1. The uncertainties quoted are standard deviations.

Table 1. Strain rate components of 22 subnets in the southern Taiwan GPS Network (1990-1994).

NET	LOCATION	$\dot{E}_{11}$ (μ strain/yr)	$\dot{E}_{12}$ (μ strain/yr)	$\dot{E}_{22}$ (μ strain/yr)
A	Penghu-SW Coast	-0.02±0.02	-0.00±0.01	-0.03±0.03
B	N. Coastal Plain	-0.24±0.04	-0.05±0.03	-0.08±0.04
C	S. Coastal Plain	-0.48±0.06	0.03±0.04	0.09±0.04
D	N. Chukou Fault	-0.34±0.05	0.30±0.04	-0.00±0.06
E	MN. Chukou Fault	-0.70±0.06	0.31±0.04	-0.02±0.04
F	MS. Chukou Fault	-1.20±0.07	0.39±0.05	0.18±0.06
G	S. Chukou Fault	-1.59±0.09	0.32±0.09	0.24±0.06
H	N. Western Foothills	-0.29±0.04	0.19±0.04	-0.01±0.04
I	M. Western Foothills	-0.25±0.05	0.21±0.03	0.16±0.04
J	S. Western Foothills	-0.27±0.04	0.15±0.03	0.10±0.03
K	Pingtung Plain	-0.33±0.06	0.19±0.03	-0.01±0.04
L	N. Central Range	0.04±0.03	0.15±0.04	-0.39±0.05
M	M. Central Range	0.41±0.03	0.14±0.03	0.02±0.04
N	S. Central Range	0.59±0.03	0.12±0.03	-0.05±0.04
O	Hengchun Peninsula	0.55±0.06	0.22±0.04	-0.11±0.02
P	N. Longitudinal Valley	-1.77±0.33	2.04±0.14	-1.50±0.08
Q	M. Longitudinal Valley	-3.38±0.23	3.33±0.14	-2.09±0.10
R	S. Longitudinal Valley	-2.81±0.19	1.04±0.09	-0.12±0.08
S	N. Coastal Range	-0.79±0.17	1.38±0.09	-0.74±0.11
T	M. Coastal Range	0.11±0.08	0.59±0.06	-0.38±0.07
U	S. Coastal Range	0.01±0.07	0.17±0.04	-0.14±0.04
V	Lutao-Lanhsu to SE.Coast	-0.48±0.03	0.24±0.02	-0.12±0.03

The strain rates are referred to a coordinate system with axis 1 directed east and axis 2 directed north. The uncertainties quoted are standard deviations. 1 μ strain = 10^{-6}

$\dot{E}_{11}$ and $\dot{E}_{22}$ are the rates of change of length per unit length in the east-west and north-south directions, respectively. The extension is reckoned as positive, while the contraction is negative in value. The $\dot{E}_{11}$ of Nets A, L, T, and U do not differ from zero at the 95% confidence level. Nets M, N, and O show significant extension in the east-west direction. In contrast, the other 15 nets all give remarkable contraction in the E-W direction. The $\dot{E}_{22}$ of Nets A, D, E, H, K, M, N, and R are not significant. Nets B and C are only marginally significant in terms of contraction and extension in the north-south direction, respectively. Nets F, G, I, and J indicate slight extension in the N-S direction. The other 8 Nets L, O, P, Q, S, T, U, and V located in the eastern part of the collision zone show very significant contraction in the N-S direction. The tensor component $\dot{E}_{12}$ represents the rate of tensor shear across any line parallel to the axis 1 (E-W direction), positive for the right-lateral shear or that for any line parallel to axis 2 (N-S direction), but positive for the left-lateral shear. Except for the three Nets A, B, and C in the westernmost part of the GPS network showing no significant values of $\dot{E}_{12}$, the other 19 nets all have remarkable positive values of $\dot{E}_{12}$. This reveals that the right-lateral shear in the E-W direction or left-lateral shear in the N-S direction are dominant within the deformation zone of the Taiwan arc-continent collision.

The average principal strain rates can be computed from three components of the surface strain rate tensor using the following formula:

$$\dot{\varepsilon}_{1,2} = \frac{1}{2}(\dot{E}_{11} + \dot{E}_{22}) \pm [\dot{E}_{12}^2 + \frac{1}{4}(\dot{E}_{11} - \dot{E}_{22})^2]^{1/2} \tag{5}$$

where $\dot{\varepsilon}_1$ and $\dot{\varepsilon}_2$ are the algebraically larger and smaller principal strain rates, respectively. The azimuth of $\dot{\varepsilon}_1$, ϕ, is found by:

$$\phi = \frac{1}{2}tan^{-1}\frac{2\dot{E}_{12}}{\dot{E}_{22} - \dot{E}_{11}} \tag{6}$$

The average principal strain rates for each of the 22 subnets are given in Table 2 and are also shown in Figure 4. All uncertainties quoted are ± 1 standard deviation. The strain rates are given in units of microstrain per year (1 μstrain = 10^{-6}). Positive values denote extension, while negative values represent contraction or shortening.

There is no significant deformation in the Penghu-SW coastal area (Net A). Slight contractions of 0.26-0.48 μstrain/yr in 73°-93° (ϕ+90°) directions are observed in the Coastal Plain (Nets B and C). In the vicinity of the Chukou fault (Nets D, E, F, and G) remarkable contractions of 0.51-1.65 μstrain/yr in the directions of 100°-120° are detected. There are also slight extensions of 0.10-0.29 μstrain/yr in the direction perpendicular to that of the contractions. The shortening rates along the surrounding region of the Chukou fault increase southward from 0.51 μstrain/yr in the northernmost section to 1.65 μstrain/yr in the southernmost section. On the other hand, the directions of maximum contraction decrease southward from 120° to 100°. The four Nets H, I, J, and K mostly in the eastern part of the Western Foothills show moderate contractions of 0.32-0.42 μstrain/yr in 109°-117° and small extensions of 0.06-0.24 μstrain/yr in 19°-27°. The northern Central Range, Net L, gives a significant shortening of 0.44 μstrain/yr in 163° and a small extension of 0.09 μstrain/yr in 73°. In contrast, the other three Nets M, N, O in the middle and southern Central Range as well as the Hengchun Peninsula indicate essentially uniaxial extensions of 0.46-0.62 μstrain/yr in the directions of 72°-80°.

Table 2. Principal strain rates of 22 subnets in the southern Taiwan GPS Network (1990-1994)

NET	LOCATION	$\dot{\varepsilon}_1$ (μ strain/yr)	$\dot{\varepsilon}_2$ (μ strain/yr)	ϕ (°)
A	Penghu-SW Coast	-0.02± 0.02	-0.03± 0.03	-88±45
B	N. Coastal Plain	-0.06±0.04	-0.26± 0.04	-17± 9
C	S. Coastal Plain	0.09± 0.04	-0.48± 0.06	3± 4
D	N. Chukou Fault	0.18 ±0.04	-0.51± 0.06	30± 4
E	MN. Chukou Fault	0.10± 0.04	-0.82± 0.06	22± 3
F	MS. Chukou Fault	0.29 ±0.05	-1.30± 0.07	15± 2
G	S. Chukou Fault	0.29± 0.05	-1.65± 0.10	10± 3
H	N. Western Foothills	0.09± 0.05	-0.39± 0.04	27± 4
I	M. Western Foothills	0.24± 0.04	-0.34± 0.04	23± 4
J	S. Western Foothills	0.15± 0.03	-0.32± 0.05	19± 3
K	Pingtung Plain	0.07± 0.04	-0.42± 0.05	25± 4
L	N. Central Range	0.09± 0.03	-0.44± 0.04	73± 4
M	M. Central Range	0.46± 0.03	-0.03± 0.04	72± 3
N	S. Central Range	0.61± 0.03	-0.10± 0.04	77± 2
O	Hengchun Peninsula	0.52± 0.07	-0.18± 0.02	71± 2
P	N. Longitudinal Valley	0.41± 0.12	-3.68± 0.29	43± 2
Q	M. Longitudinal Valley	0.66± 0.09	-6.12± 0.26	40± 1
R	S. Longitudinal Valley	0.24± 0.06	-3.17± 0.20	19± 2
S	N. Coastal Range	0.61± 0.10	-2.14± 0.15	44± 2
T	M. Coastal Range	0.50± 0.06	-0.77± 0.09	56± 3
U	S. Coastal Range	0.12± 0.07	-0.25± 0.04	57± 7
V	Lutao-Lanhsu to SE. Coast	-0.01± 0.03	-0.60± 0.03	27± 2

The extremely high shortening rates of 3.2-6.1 μstrain/yr in 109°-133° are observed in the Longitudinal Valley area, Nets P, Q, and R. Moderate extensions of 0.24-0.66 μstrain/yr in 19°-43° are also found. These results are similar to those reported by Yu and Lee (1986) and Yu and Yu (1991) based on repeated trilateration data. The high strain rates in the Longitudinal Valley area are obviously caused by the rapid aseismic slip on the Longitudinal Valley fault (LVF) and the small-aperture of the geodetic network. The northern Coastal Range (Net S) gives similar high strain rates and direction as those in the northern Longitudinal Valley (Net P). We suspect that two stations, S076 and 1047, located in the western margin of the Coastal Range may belong to the western side of the LVF (see Figure 1). Thus, the rapid shortening is likely to have been caused by the slip on the LVF. However, this inference still needs to be verified. The strain rates in the middle and southern Coastal Range are also significant with 0.25-0.77 μstrain/yr contractions in 146°-147° and 0.12-0.50 μstrain/yr extensions in 56°-57°. The offshore area from Lutao-Lanhsu to the southeastern coast shows a remarkable uniaxial contraction of 0.60 μstrain/yr in the direction of 117°. The active LVF may extend southward as revealed by the detailed geophysical studies off southeastern Taiwan (Huang et al., 1992). Thus, the high strain rate in the area may be partly due to a slip on the fault.

6. VELOCITY FIELD OF GEODETIC STATIONS

6.1 Rate of Length Change

The average rates of length change on each baseline are determined by linear regression on time. The positive value of length rate represents extension, while the negative rate of length change denotes shortening. The standard errors of the average rates are also estimated based on the residuals to the best linear fittings. Table 3 shows the average rates of length change for baselines in two profiles across the Taiwan arc-continent collision zone. The upper numbers between two stations (e.g. S01R and S004) are average rates of length change in units of mm/yr. The uncertainties quoted are standard deviations. The lower numbers are baseline lengths in meters. Profile 1 is composed of 9 baselines and extends from Paisha, Penghu (S01R) southeasterly to Lutao (S063) with a total length of 223 km (see Figure 1). Between stations S01R and S004, no significant change of baseline length is detected. From station S004 to station 7205, a summing up of 41.4±3.9 mm/yr shortening is observed and about half of it occurs across the Chukou fault (S007-S066). Baseline 7205-S045, which covers the Central Range, gives a 8.6±2.8 mm/yr extension. The short baseline S045-0207 traverses the Longitudinal Valley and indicates a 29.6±5.6 mm/yr contraction which is very close to that observed from trilateration surveys (Yu *et al.*, 1992). Within the Coastal Range (0207-S054), the deformation is negligible. Between S054 and S063 (Lutao) a significant contraction of 19.3±5.7 mm/yr is seen. In total, Profile 1 gives a remarkable shortening rate of 78.7±10.1 mm/yr.

Table 3. Average rates of length changes for baselines in two profiles across the Taiwan arc-continent collision zone.

Profile 1. Paisha , Penghu - Lutao

S01R	$\dfrac{2.4\pm2.1}{67985\ m}$	S004	$\dfrac{-11.6\pm2.9}{24448\ m}$	S007	$\dfrac{-20.0\pm2.1}{14835\ m}$	S066	$\dfrac{-4.2\pm1.0}{12952\ m}$	S065
S065	$\dfrac{-5.6\pm1.3}{16640\ m}$	7205	$\dfrac{8.6\pm2.8}{38863\ m}$	S045	$\dfrac{-29.6\pm5.6}{9770\ m}$	0207	$\dfrac{0.6\pm3.2}{5773\ m}$	S054
S054	$\dfrac{-19.3\pm5.7}{32230\ m}$	S063		S063	$\dfrac{0.7\pm1.7}{51400\ m}$	S102		

Profile 2. Chimei , Penghu - Lanhsu

S002	$\dfrac{-16.2\pm3.3}{86223\ m}$	I004	$\dfrac{-8.8\pm1.2}{28518\ m}$	0621	$\dfrac{-11.6\pm3.4}{23886\ m}$	S23R	$\dfrac{4.8\pm3.4}{38888\ m}$	S043
S043	$\dfrac{-51.9\pm4.8}{80256\ m}$	S102		S002	$\dfrac{1.6\pm2.8}{69958\ m}$	S01R		

* The upper numbers between two stations (e.g. S01R and S004) are average rates of length changes in units of mm/yr. The uncertainties quoted are standard deviations. The lower numbers are baseline lengths in meters

Profile 2 consists of only 5 baselines and extends from Chimei, Penghu (S002) south-easterly to Lanhsu (S102) with a sum total 258 km in length. The significant contraction of 16.2±3.3 mm/yr between Chimei (S002) and Tainan (I004) is unexpected. From I004, through 0621 to S23R, which covers the Western Foothills and Pingtung Plain, there is a 20.4±3.6 mm/yr shortening. The distribution of crustal strain to the west of the Central Range seems to be somewhat different in two profiles. In the Central Range a small extension of 4.8±3.4 mm/yr is found on baseline S23R-S043. However, a tremendous shortening rate of 51.9±4.8 mm/yr is observed between S043 and S102 (Lanhsu). It is approximately the sum of the contraction in the Longitudinal Valley (29.6±5.6 mm/yr) and that between S054 and Lutao (19.3±5.7 mm/yr) in the Profile 1. The Profile 2 shows a total shortening rate of 83.4±7.6 mm/yr. Two baselines, S063-S102 and S002-S01R, connecting these two profiles reveal no significant change in length.

6.2 Relative Station Velocity

The individual values of the average length rate for all of the observed baselines are weighted by the reciproccal square of the standard deviation in the rate. These weighted rates are then used in a least squares adjustment to estimate the relative velocities of geodetic stations in the southern Taiwan GPS Network (Prescott, 1981). Eight fixed continuous-monitoring GPS stations (solid triangles inside circle in Figure 1) at Paisha (S01R), Pingtung (S23R), Taipei (T986), Lanhsu (S102), Changping (S058), Minhsiung (S103), Fushan (S104), and Mingyeh (S105) have been operated by the Institute of Earth Sciences, Academia Sinica since November 1991 (Yu and Kuo, 1993). The estimated average rates of length change for baselines between these fixed GPS stations are also incorporated with those from mobile stations in the estimation of relative station velocities. The average rates of change on the east and north components for the baseline between Paisha and Taipei (S01R-T986) are 0.5±1.0 mm/yr and 1.0±0.4 mm/yr, respectively. In other words, the relative motion between stations S01R and T986 is not significant. Based on this fact and the relatively geological stablility in the Penghu area, we fix the coordinates of station S01R and the azimuth from S01R to T986 in the least-squares adjustment to estimate the station velocities. This proceduce is necessary for resolving the translation and rotational ambiguities of the whole network. The estimated velocities of all stations relative to station S01R are plotted in Figure 5. The 95% confidence ellipse is also shown at the tip of each velocity vector.

The station velocity vectors in eastern Taiwan trend in NW-WNW directions then gradually to the west in the Western Foothills. In the Kaohsiung-Pingtung coastal area, it is even directed toward the southwest. The velocities for stations in the Coastal Plain are only marginally significant. This pattern of velocity field in the arc-continent collision zone is consistent with the trends of present-day maximum compressional stress axes inferred from borehole breakout data (Suppe *et al.*, 1985) and analyses of groups of earthquake focal mechanisms (Yeh *et al.*, 1991). The present-day horizontal maximum stress axes in Taiwan determined from these sources generally show a fan-shaped distribution (Hu *et al.*, 1994). It is dominated by NE-SW compression which is mainly due to the arc-continent collision. The paleostresses determined from tectonic analyses of fault-slip data in Quaternary formations also show a similar fan-shaped pattern (Angelier *et al.*, 1986; Angelier *et al.*, 1990).

Table 4 gives the relative velocities of stations in five profiles. Profiles 1 and 2 show NW-SE trending and extend from Paisha and Chimei, Penghu to Lutao and Lanhsu, respectively, as previously described. Profile 3 starts from Lanhsu and Lutao, then continues along

the eastern coast northerly to Fengping (S077). Profile 4 runs along the western margin of the Coastal Range, while Profile 5 extends from the southernmost tip of Taiwan Island northerly along the eastern margin of the Central Range. Traversing the arc-continent collision zone, Profiles 1 and 2 clearly show an eastward increase in the magnitudes and azimuths of the velocity vectors. The velocities relative to S01R in the western Coastal Plain (S004 and I004) are 8.6±2.8 and 9.5±3.3 mm/yr, respectively. At the volcanic islands of the Philippine Sea plate, Lutao and Lanhsu, the relative velocities are 78.3±4.3 and 86.3±2.4 mm/yr, respectively. Across the Chukou fault (from S007 to S066) and Longitudinal Valley (S045 to 0207), there are big discontinuities of 17.4 and 31.7 mm/yr on the velocities. We have realized that the discontinuity in the Longitudinal Valley is mainly caused by the aseismic slip on the LVF (Yu and Liu, 1989; Yu *et al.*, 1990). On the other hand, whether the 17.4 mm/yr's discontinuity across the Chukou fault is due to fault-slip or not needs to be further studied.
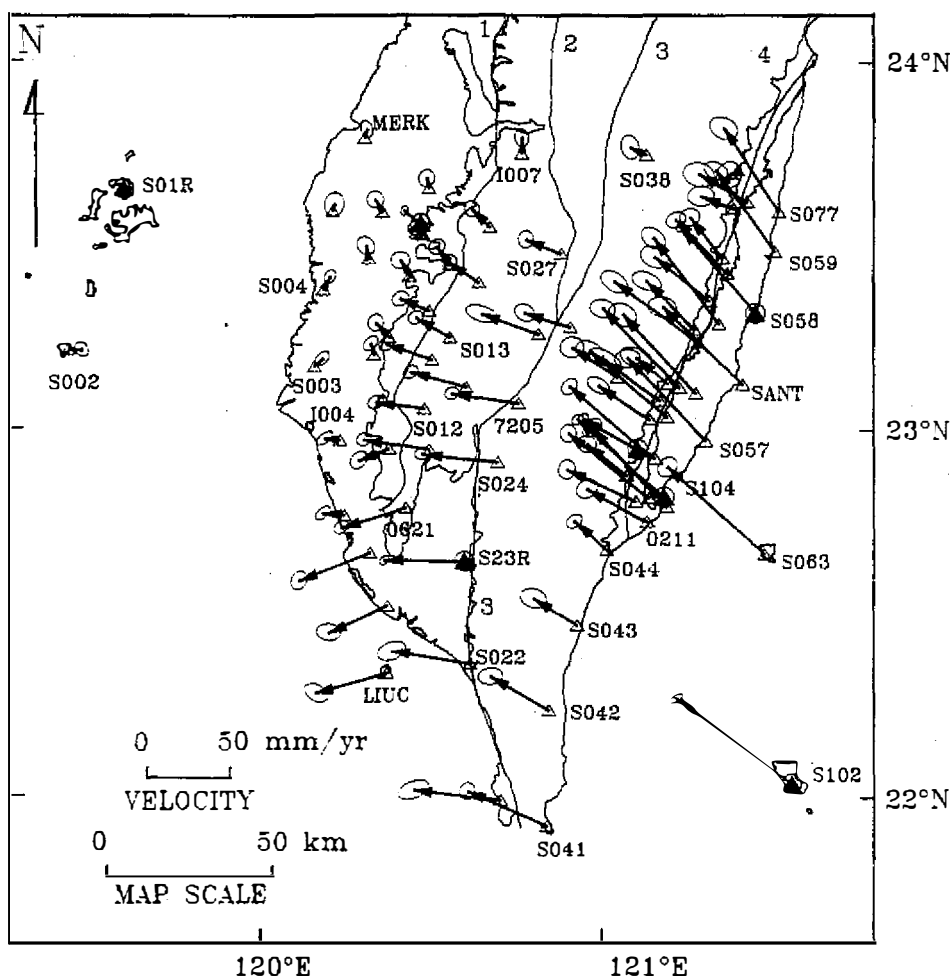

Fig. 5. Velocities of stations relative to Paisha (S01R). The 95% confidence ellipse is shown at the tip of each velocity vector.

Table 4. Relative velocities of stations in five profiles estimated from
1990-1994 GPS data.

Profile 1. Paisha , Penghu - Lutao

Station	V_x(mm/yr)	V_y(mm/yr)	V(mm/yr)	Azimuth($°$)
S01R	Fixed	Fixed	Fixed	Fixed
S004	3.9±1.8	7.7±2.1	8.6±2.8	26±12
S007	-8.3±2.4	8.9±2.5	12.2±3.5	317±12
S066	-27.9±2.3	10.0±2.0	29.6±3.1	290± 4
S065	-33.9±2.3	8.8±1.9	35.0±3.0	285± 3
7205	-40.2±2.1	6.4±1.8	40.7±2.8	279± 3
S045	-23.9±3.0	18.4±2.6	30.2±4.0	308± 5
0207	-48.3±2.5	38.7±2.7	61.9±3.7	309± 2
S054	-44.5±2.9	47.5±2.9	65.1±4.1	317± 3
S063	-58.2±3.0	52.3±3.1	78.3±4.3	312± 2

Profile 2. Chimei , Penghu - Lanhsu

S002	7.8±2.0	-0.1±2.2	7.8±3.0	91±16
I004	-9.5±2.5	0.8±2.1	9.5±3.3	275±13
0621	-39.2±2.3	-11.9±2.0	41.0±3.1	253± 3
S23R	-48.1±1.4	0.7±1.4	48.1±2.0	271± 2
S043	-29.3±3.9	17.9±3.0	34.3±4.9	301± 5
S102	-69.2±1.9	51.5±1.5	86.3±2.4	307± 1

Profile 3. Lanshu , Lutao , and Eastern Coast

S102	-69.2±1.9	51.5±1.5	86.3±2.4	307±1
S063	-58.2±3.0	52.3±3.1	78.3±4.3	312±2
S054	-44.5±2.9	47.5±2.9	65.1±4.1	317±3
S104	-51.2±1.8	46.7±1.6	69.3±2.4	312±1
S057	-45.9±3.9	50.0±2.8	67.9±4.8	317±3
SANT	-47.6±4.3	46.9±3.2	66.8±5.4	315±3
S058	-44.1±1.2	52.4±1.5	68.5±1.9	320±1
S059	-34.7±3.6	49.0±2.8	60.0±4.6	325±3
S077	-32.8±4.3	50.3±3.5	60.1±5.5	327±4

Table 4. (Continued)

Profile 4. Western Margin of the Coastal Range

Station	V_x(mm/yr)	V_y(mm/yr)	V(mm/yr)	Azimuth(°)
0207	-48.3±2.5	38.7±2.7	61.9±3.7	309±2
S072	-50.9±2.4	43.0±2.6	66.6±3.5	310±2
S056	-46.0±4.2	40.2±3.2	61.1±5.3	311±3
S033	-43.0±4.3	47.5±3.5	64.1±5.5	318±4
0283	-45.6±3.9	47.9±2.8	66.1±4.8	316±3
S073	-49.2±4.1	37.0±3.5	61.6±5.4	307±3
0135	-38.2±3.5	51.9±3.3	64.4±4.8	324±3
1047 *	-30.7±2.9	32.6±2.5	44.8±3.8	317±3
S076 *	-28.4±4.7	16.7±3.7	33.0±6.0	300±7

Profile 5. Eastern Margin of the Central Range

Station	V_x(mm/yr)	V_y(mm/yr)	V(mm/yr)	Azimuth(°)
S041	-48.3±2.3	21.1±2.8	52.7±3.6	294±3
S042	-34.5±3.7	19.8±2.6	39.8±4.5	300±4
S043	-29.3±3.9	17.9±3.0	34.3±4.9	301±5
S044	-19.4±2.5	16.8±2.1	25.7±3.3	311±5
S045	-23.9±3.0	18.4±2.6	30.2±4.0	308±5
S105	-32.1±1.6	17.9±1.7	36.8±2.3	299±3
S040	-32.0±3.4	21.1±2.5	38.3±4.2	303±4
S039	-27.7±4.3	28.9±3.0	40.0±5.2	316±5
0201	-32.1±4.0	26.4±3.4	41.6±5.3	309±5
S047	-19.5±3.0	24.7±2.7	31.5±4.0	322±5

* Station probably belongs to the western side of the Longitudinal Valley fault

Profiles 3 and 4 show the relative velocities of stations located in the Coastal Range and two offshore islands, Lutao and Lanhsu, except two stations, 1047 and S076, which probably belong to the western side of the LVF. The velocities of the latter stations, 1047 and S076, are clearly different from those of the other stations in the Coastal Range and seem to be more closely related to those of the stations in the Central Range. The station velocities in Profiles 3 and 4 (except for 1047 and S076) range from 60±4.6 mm/yr at S059 to 86.3±2.4 mm/yr at S102 (Lanhsu). From south to north, the azimuths of velocity vectors increase in a more northerly direction. It is likely to have been caused by the blockage of the competent Central Range in the collision process. A similar phenomenon of changing moving directions was also reported by Yu *et al.* (1990) from trilateration data. The observation of faster velocities at Lutao and Lanhsu than those in the Coastal Range indicates that there is a significant deformation in the margin of the Philippine Sea plate. This GPS observed moving velocity of the Philippine Sea plate relative to the Eurasian plate near Taiwan is about 15-20% faster than that estimated by Seno (1977) or Seno *et al.* (1993) which are 70 mm/yr and 73 mm/yr respectively. The velocities for stations along the eastern margin of the Central Range (Profile 5) are in the range of 32-53 mm/yr with no systematic changes in magnitudes or azimuths.

7. CONCLUSIONS

The southern Taiwan GPS Network is composed of 78 stations, seven of which are continuous-monitoring fixed GPS stations. It extends from two islets, Paisha and Chimei, Penghu situated on the Chinese continental margin, southeastly to the two volcanic islands of the Luzon arc, Lutao and Lanhsu, offshore of Taitung. This 270 km wide network has been surveyed 5 times from 1990 to 1994. Analyzing these repeated GPS data, we evaluate the precision of our GPS measurements and study the spatial variation of the crustal strain over the Taiwan arc-continent collision zone. We also estimate the horizontal velocity field of the whole network. The results are summarized as follows:

(1) Following Davis *et al.* (1989) we define the repeatability of a baseline component or length as the weighted root-mean-square scatter about its linear trend. The precision of our GPS measurements as a function of the baseline length can be described by:

$$\sigma_L = \left(a^2 + b^2 \cdot L^2 \right)^{1/2}$$

where σ_L is the standard deviation, L is the baseline length. Best fitting curves through the repeatability data for all of the observed baselines give a= 5.4±0.2 mm, 5.0±0.2 mm, 6.6±0.3 mm, 22.1±1.1 mm, and b= 0.06±0.01 ppm, 0.07±0.01 ppm, 0.09±0.02 ppm, 0.31±0.04 ppm for length and north, east and vertical components respectively. Thus the standard deviations of the lengths range from 5 to 9 mm for the baseline of 3-120 km used in this study.

(2) The whole network is divided into 22 subnets for assessing the spatial variation of the crustal strain. The average strain rates in the Penghu-SW coastal area are not significant. Slight contractions of 0.26-0.48 μstrain/yr in 73°-117° are observed in the Coastal Plain and the eastern part of the Western Foothills. The uniaxial extension of 0.46-0.62 μstrain/yr in 72°-80° is found in the southern Central Range and the Hengchun Peninsula.

(3) Remarkable contractions of 0.51-1.65 μstrain/yr in 100°-120° and small extensions of 0.10-0.29 μstrain/yr in 10°-30° are detected in the vicinity of the Chukou fault. The shortening rates increase southward along the fault, while their azimuths decrease.

(4) Due to the rapid aseismic slip on the Longitudinal Valley fault (LVF), the Longitudinal Valley area gives extremely high shortening rates of 3.2-6.1 μstrain/yr in 109°-133°, which reach a similar result to that from trilateration data.

(5) Moderate contractions of 0.25-0.77 μstrain/yr in 146°-147° and extensions of 0.12-0.50 μstrain/yr in 56°-57° are observed in the Coastal Range. The offshore area between Lutao-Lanhsu and the SE coast shows a remarkable uniaxial contraction of 0.60 μstrain/yr in 117°.

(6) Two profiles traversing the arc-continent collision zone and extending from Paisha, Penghu to Lutao and from Chimei, Penghu to Lanhsu give the total shortening rates of 78.7±10.1 mm/yr and 83.4±7.6 mm/yr, respectively.

(7) The velocity field of the geodetic stations estimated from the average rates of length change for all of the observed baselines shows a fan-shaped pattern, which is consistent with the directions of maximum compressional tectonic stress inferred from the earthquake focal mechanisms, borehole breakout data, and microtectonic analysis of Quaternary fault-slip data.

(8) In the Coastal Range, the station velocities are 60.0-69.3 mm/yr in 309°-327°, while the moving velocities at Lutao and Lanhsu are 78.3 mm/yr in 312° and 86.3 mm/yr in 307°, respectively. These obvious differences in station velocities indicate that there is a significant deformation on the margin of the Philippine Sea plate.

(9) About 31.7 mm/yr discontinuity on the velocity field across the Longitudinal Valley has been recognized as being related to the aseismic slip of the LVF as previously demonstrated by trilateration data. However, whether the velocity discontinuity of 17.4 mm/yr across the Chukou fault is due to fault-slip or mainly to strain accumulation requires further study.

(10) The velocity of Lanhsu (S102) relative to Paisha (S01R), 86.3±2.4 mm/yr in 307°±1°, may be considered the lower bound of the Philippine Sea plate's moving velocity relative to the Eurasian plate since there is probably little deformation to the west of Paisha, Penghu or to the east of Lanhsu. This GPS observed plate velocity near Taiwan is almost in the same direction as that estimated by Seno (1977) and Seno et al. (1993), but the rate is about 15-20% faster. Based on the GPS observations over only a 4 years period, it has been determined that the arc-continent collision affects almost the whole width of the Island of Taiwan, i.e., the deformation zone is at least 200 km in width. Further measurements in the next 5-10 years will provide more reliable data for the study of the crustal deformation in the collision zone.

REFERENCES

Angelier, J., F. Bergerat, H. T. Chu, and T. Q. Lee, 1990: Tectonic analysis and the evolution of a curved collision belt: the Hsüehshan Range, northern Taiwan. *Tectonophysics*, **183**, 77-96.

Barrier, E., J. Angelier, H. T. Chu, and L. S. Teng, 1982: Tectonic analysis of compressional structure in an active collision zone: the deformation of Pinanshan Conglomerates, eastern Taiwan. *Proc. Geol. Soc. China*, **25**, 123-138.

Barrier, E., and J. Angelier, 1986: Active collision in eastern Taiwan: the Coastal Range. *Tectonophysics*, **125**, 39-72.

Biq, C. C., 1972: Dual trench structure in the Taiwan-Luzon region. *Proc. Geol. Soc. China*, **15**, 65-75.

Blewitt, G., 1989: Carrier-phase ambiguity resolution for the Global Positioning System applied to geodetic baselines up to 2000 km. *J. Geophys. Res.*, **94**, 10187-10203.

Bowin, C., R. S. Lu, C. S. Lee, and H. Schouten, 1978: Plate convergence and accretion in the Taiwan-Luzon region. *Am. Assoc. Petrol. Geol. Bull.*, **62**, 1645-1672.

Brunner, F. K., and W. M. Welsch, 1993: Effects of the troposphere on GPS measurements. *GPS World*, **4**, 42-51.

Davis, J. L., W. H. Prescott, J. L. Svarc, and K. Wendt, 1989: Assessment of Global Positioning System measurements for studies of crustal deformation. *J. Geophys. Res.*, **94**, 13635-13650.

DeMets, C. R., R. G. Gordon, D. Argus, and S. Stein, 1990: Current plate motions. *Geophys. J. Inter.*, **101**, 425-478.

Dixon, T. H., 1991: An introduction to the Global Positioning System and some geological applications. *Rev. Geophysics*, **29**, 249-276.

Dong, D., and Y. Bock, 1989: GPS network analysis with phase ambiguity resolution applied to crustal deformation studies in California. *J. Geophys. Res.*, **94**, 3949-3966.

Goad, C., 1993: IGS orbit comparisons. Proc. 1993 IGS Workshop, Berne, Switzerland, 218-225.

Herring, T. A., 1986: Precision of vertical position estimates from very long baseline interferometry. *J. Geophys. Res.*, **91**, 9177-9182.

Ho, C. S., 1976: Foothills tectonics of Taiwan. *Bull. Geol. Surv. Taiwan*, **25**, 9-28.

Ho, C. S., 1982: Tectonic evolution of Taiwan.: Explanatory text of the tectonic map of Taiwan, Ministry of Economic Affairs, R.O.C., 126pp.

Ho, C. S., 1986: A synthesis of the geologic evolution of Taiwan. *Tectonophysics*, **125**, 1-16.

Hopfield, H. S., 1971: Tropospheric effect on electromagnetically measured range: Prediction from surface weather data. *Radio Sci.*, **6**, 357-367.

Hsu, T. L., 1976: Neotectonics of the Longitudinal Valley, eastern Taiwan. *Bull. Geol. Surv. Taiwan*, **25**, 53-62.

Huang, T. C., 1978: Calcareous nannoplankton, paleoenvironment, age, and correlation of the upper Wulai Group and the lower Hsichih Group (Oligocene to Miocene) in northern Taiwan. *Proc. Geol. Soc. China*, **21**, 128-150.

Huang, T. C., 1980: Oligocene to Pleistocene calcareous nannofossil biostratigraphy of the Hsuehshan Range and western foothills in Taiwan. *Geol. and Paleont. SE Asia*, Univ. of Tokyo Press, **21**, 191-210.

Huang, C. Y., C. T. Shyu, S. B. Lin, T. Q. Lee, and D. D. Sheu, 1992: Marine geology in the arc-continent collision zone off southeastern Taiwan: Implications for late Neogene evolution of the Coastal Range. *Marine Geology*, **107**, 183-212.

Hu, J. C., J. Angelier, J. C. Lee, H. T. Chu, and D. Byrne, 1994: Kinematics of convergence, deformation and stress distribution in the Taiwan collision area: 2-D finite-element numerical modelling. *Tectonophysics* (in press).

Jackson, D. D., and M. Matsu'ura, 1985: A Bayesian approach to nonlinear inversion. *J. Geophys. Res.*, **90**, 581-591.

Kuo, L. C., S. B. Yu, and C. S. Chen, 1994: A study on the processing strategies of continuous GPS data. Proc. 13th Conference of Surveying and Its Applications, Hsinchu, Taiwan, R.O.C., 121-131 (in Chinese).

Lu, C. Y., and J. Malavieille, 1994: Oblique convergence, indentation and rotation tectonics in the Taiwan Mountain Belt: Insights from experimental modelling. *Earth Planet. Sci. Lett.*, **121**, 477-494.

Prescott, W. H., 1981: The determination of displacement fields from geodetic data along a strike-slip fault. *J. Geophys. Res.*, **86**, 6067-6072.

Prescott, W. H., J. C. Savage, and W. T. Kinoshita, 1979: Strain accumulation rates in the western United States between 1970 and 1978. *J. Geophys. Res.*, **84**, 5423-5435.

Savage, J. C., and W. H. Prescott, 1973: Precision of Geodolite distance measurements. *J. Geophys. Res.*, **78**, 6001-6008.

Seno, T., 1977: The instantaneous rotation vector of the Philippine Sea plate relative to the Eurasian plate. *Tectonophysics*, **42**, 209-226.

Seno, T., S., Stein and A.E. Gripp, 1993: A model for the motion of the Philippine Sea plate consistent with NUVEL-1 and geological data. *J. Geophys. Res.*, **98**, B17941-B17948.

Suppe, J., 1980: Imbricate structure of western foothills belt, south-central Taiwan. *Petrol. Geol. Taiwan*, **17**, 1-16.

Suppe, J., 1981: Mechanics of mountain building and metamorphism in Taiwan. *Mem. Geol. Soc. China*, **4**, 67-89.

Suppe, J., C. T. Hu, and Y. J. Chen, 1985: Present-day stress direction in western Taiwan inferred from borehole elongation. *Petrol. Geol. Taiwan*, **21**, 1-12.

Tralli, D. M., and T. H. Dixon, 1988: A few parts in 10^8 geodetic baseline repeatability in the Gulf of California using the Global Positioning System. *Geophys. Res. Lett.*, **15**, 353-356.

Tsai, Y. B., 1986: Seismotectonics of Taiwan. *Tectonophysics*, **125**, 17-37.

Tsai, Y. B., T. L. Teng, J. M. Chiu, and H. L. Liu, 1977: Tectonic implications of the seismicity in the Taiwan region. *Mem. Geol. Soc. China*, **2**, 13-41.

Willians, C. R., T. Arnadottir, and P. Segall, 1993: Coseismic deformation and dislocation models of the 1989 Loma Prieta earthquake derived from Global Positioning System measurements. *J. Geophys. Res.*, **98**, 4567-4578.

Wu, F. T., 1978: Recent tectonics in Taiwan. *J. Phys. Earth*, **26**, S265-S299.

Yeh, Y. H., E. Barrier, C .H. Lin, and J. Angelier, 1991: Stress tensor analysis in the Taiwan area from focal mechanisms of earthquakes. *Tectonophysics*, **200**, 276-280.

Yu, S. B., and Y. B. Tsai, 1982: A study of microseismicity and crustal deformation of the Kuangfu-Fuli area in eastern Taiwan. *Bull. Inst. Earth Sci., Academia Sinica*, **2**, 1-18.

Yu, S. B., and C. Lee, 1986: Geodetic measurement of horizontal crustal deformation in eastern Taiwan. *Tectonophysics*, **125**, 73-85.

Yu, S. B., and C. C. Liu, 1989: Fault creep on the central segment of the Longitudinal Valley fault, eastern Taiwan. *Proc. Geol. Soc. China*, **32**, 209-231.

Yu, S. B., D. D. Jackson, G. K. Yu, and C. C. Liu, 1990: Dislocation model for crustal deformation in the Longitudinal Valley area, eastern Taiwan. *Tectonophysics*, **183**, 97-109.

Yu, S. B., and G. K. Yu, 1991: Present-day crustal deformation in the Longitudinal Valley area, eastern Taiwan. TAICRUST Workshop Proc., Taipei, Taiwan, R.O.C., 185-195.

Yu, S. B., G. K., Yu, L. C. Kuo, and C. Lee, 1992: Crustal deformation in the southern Longitudinal Valley area, eastern Taiwan. *J. Geol. Soc. China*, **35**, 219-230.

Yu, S. B., and L. C. Kuo, 1993: Utilizing continuous GPS data to study the crustal deformation in Taiwan. *Bull. Inst. Earth Sci., Academia Sinica*, **13**, 77-82.